

Dark Photon Dark Matter from Cosmic Strings and Gravitational Wave Background

Naoya Kitajima^(a,b) and Kazunori Nakayama^(b,c)

^(a)*Frontier Research Institute for Interdisciplinary Sciences, Tohoku University, Sendai 980-8578, Japan*

^(b)*Department of Physics, Tohoku University, Sendai 980-8578, Japan*

^(c)*International Center for Quantum-field Measurement Systems for Studies of the Universe and Particles (QUP), KEK, 1-1 Oho, Tsukuba, Ibaraki 305-0801, Japan*

Abstract

Dark photon dark matter may be produced by the cosmic strings in association with the dark U(1) gauge symmetry breaking. We perform three-dimensional lattice simulations of the Abelian-Higgs model and follow the evolution of cosmic strings. In particular, we simulate the case of (very) light vector boson and find that such vector bosons are efficiently produced by the collapse of small loops while the production is inefficient in the case of heavy vector boson. We calculate the spectrum of the gravitational wave background produced by the cosmic string loops for the light vector boson case and find characteristic features in the spectrum, which can serve as a probe of the dark photon dark matter scenario. In particular, we find that the current ground-based detectors may be sensitive to such gravitational wave signals and also on-going/future pulsar timing observations give stringent constraint on the dark photon dark matter scenario.

Contents

1	Introduction	1
2	Simulation of Abelian-Higgs string networks	2
2.1	Model	2
2.2	Numerical simulation	3
3	Gravitational wave background from cosmic strings	11
3.1	Energy loss of loops	11
3.2	Loop density	12
3.3	Gravitational wave spectrum	14
4	Conclusions and discussion	19

1 Introduction

Dark photon is one of the candidates of dark matter (DM) of the Universe [1, 2]. The dark photon may have string-theoretic origins [3, 4] and phenomenologically it is characterized by the mass and coupling through the kinetic mixing with the Standard Model photon. There are several known mechanisms for the dark photon production processes in order for the dark photon to be DM: gravitational production [5–10], gravitational thermal scattering [11, 12], production through axion couplings [13–15], through Higgs couplings [16, 17] and cosmic strings [18].¹ In this paper we focus on the production through the cosmic strings.

If the dark photon, A_μ , is associated with the dark U(1) gauge symmetry, it is natural that the finite dark photon mass arises from the Higgs mechanism, where the dark Higgs field Φ obtains a vacuum expectation value (VEV) and the dark U(1) symmetry is spontaneously broken. If the symmetry breaking happens after inflation, cosmic string networks appear in the Universe as topological defects [24]. Once formed, the cosmic strings radiate dark photons if the dark photon is sufficiently light and the dark photon abundance produced in this way can be consistent with the present DM abundance [18].

One of the main purposes of our study is to confirm that the cosmic strings efficiently emit dark photons with the use of three-dimensional lattice simulation. On this point, one should note that there are already a series of studies for the case of global strings, i.e., the axion emission from cosmic strings associated with the global U(1) symmetry breaking [25–48]. An important property of the global strings is that the average string number per Hubble volume grows logarithmically with time: $\xi(t) = \beta + \alpha \log(m_r/H)$, which we call the logarithmic violation of the scaling law [40–42, 44, 45, 47]. On the other hand, Refs. [43, 46] claim the conventional scaling law: $\xi(t) = \text{const} \simeq 1$. Although these results have been obtained for

¹The misalignment production scenario [19, 20] suffers from serious instability or excluded by cosmological observations without significant modification of the cosmological models [21, 22] See also Ref. [23] for an alternative scenario.

global strings, one may expect that the production of the longitudinal vector boson should be similar to the axion thanks to the Goldstone boson equivalence theorem if the momentum is high enough. We will reveal it by an explicit calculation.

Another main purpose of this paper is to estimate the gravitational wave (GW) background spectrum in the cosmic string scenario for the dark photon DM. The estimation of GW background from the cosmic strings, in particular from cosmic string loops, have been done in many works mostly in the case of local strings [49–64]. Recently GWs from global string have been calculated in connection with the recent development of the global string simulation with the improved scaling properties [65, 66]. The inclusion of axion or vector boson (dark photon) emission drastically affects the resulting GW spectrum, since the most energy of string loops goes to the axion or dark photon emission while only tiny fraction of the loop energy is consumed as GW emission.² Even more complexity arises when the dark photon is light but has finite mass. In such a case, loops longer than some threshold cannot emit dark photon while shorter ones can emit it. Thus the cosmic strings in this scenario will be a mixture of “local-type” and “global-type” strings. Such nontrivial structures should be imprinted in the shape of the GW spectrum. Ref. [18] already pointed out such a possibility, but detailed calculations have not been performed. We show explicitly the GW spectrum as a probe of the dark photon DM scenario.

This paper is organized as follows. In Sec. 2 we perform a three-dimensional lattice simulation of the local strings with light dark photon. In Sec. 3 we estimate the GW background from the cosmic string loops in the dark photon DM scenario. In Sec. 4 we give conclusions and discussion.

2 Simulation of Abelian-Higgs string networks

In this section, we numerically show the evolution of Abelian-Higgs string networks with both local-type and near-global-type cases. First, we focus on the scaling behavior for the cosmic string length. Then, we show the emission of dark photons from the string network.

2.1 Model

Let us consider the Abelian-Higgs model in the hidden sector with the dark U(1) gauge symmetry given by the following Lagrangian,

$$\mathcal{L} = (D_\mu \Phi)^* D^\mu \Phi - \frac{1}{4} F_{\mu\nu} F^{\mu\nu} - \frac{\lambda}{4} (|\Phi|^2 - v^2)^2, \quad (1)$$

where Φ is the dark Higgs field, $D_\mu = \partial_\mu - ieA_\mu$ is the covariant derivative operator with A_μ being the dark photon field, $F_{\mu\nu} = \partial_\mu A_\nu - \partial_\nu A_\mu$ is the field strength tensor, e , λ and v are

²The cusps on the string loops may also emit high-energy particles [67, 68]. See also Refs. [69–71] where efficient dark photon/Higgs emission from local-type strings has also been reported. Phenomenology/cosmology of cosmic strings due to heavy particle radiation have been discussed in Refs. [72–77].

respectively the gauge coupling constant, the scalar self coupling constant and the vacuum expectation value. Since $|\Phi| = v$ at the minimum of the potential, the U(1) symmetry is spontaneously broken and cosmic strings are formed in association with the symmetry breaking. The equations of motion are derived as follows,

$$\frac{1}{\sqrt{-g}}D_\mu(\sqrt{-g}D^\mu\Phi) + \frac{\partial V}{\partial\Phi^*} = 0, \quad (2)$$

$$\frac{1}{\sqrt{-g}}\partial_\mu(\sqrt{-g}F^{\mu\nu}) - 2e\text{Im}(\Phi^*D^\nu\Phi) = 0. \quad (3)$$

Here and in what follows, we assume the flat Friedmann-Lemaitre-Robertson-Walker (FLRW) metric as the background spacetime and use the conformal time, τ , as time variable. In addition, we impose the temporal gauge, $A_0 = 0$, throughout this paper. The system of evolution equations can be written as

$$\Phi'' + 2\mathcal{H}\Phi' - D_iD_i\Phi + a^2\frac{\partial V}{\partial\Phi^*} = 0, \quad (4)$$

$$E'_i + \partial_jF_{ij} - 2ea^2\text{Im}(\Phi^*D_i\Phi) = 0, \quad (5)$$

$$\partial_iE_i - 2ea^2\text{Im}(\Phi^*\Phi') = 0, \quad (6)$$

where the prime denotes the derivative with respect to the conformal time, a is the scale factor, $\mathcal{H} = a'/a$, $E_i \equiv F_{0i}$ and repeated indices are summed. Note that two of these equations (Eq. (4) and (5)) determine the field dynamics and the Eq. (6) is the constraint equation corresponding to the Gauss's law. Here and in what follows, we assume the radiation-dominated universe, i.e. $a \propto \tau$ and $\mathcal{H} = 1/\tau$ and the energy density of the Abelian-Higgs system is negligible with respect to the background radiation density. Note that the dynamics depends only on the ratio $\lambda/(2e^2)$ after redefining the field values. It corresponds to the square of the ratio between the mass of the radial component of the scalar field and the mass of the dark photon $m_A = \sqrt{2}ev$ around the symmetry-breaking vacuum. Specifically, the dark photon is much lighter than the radial mode for $e^2 \ll \lambda$ and one can expect that string configuration approaches to the global string one. In the following, we numerically show the scaling behavior and emission of dark photons in both local and near-global cases. In the following numerical analysis, we set $\lambda = 2$ throughout.

2.2 Numerical simulation

One can follow the evolution of Abelian-Higgs string network by solving the system of equations (4),(5) under the constraint equation (6). In general, the dynamics of topological defects is highly nonlinear and hence we adopt three-dimensional lattice simulation.

The Abelian-Higgs lattice simulation has been performed in the literature [78–83] and we follow the formulation based on the lattice gauge theory [79]. In this formalism, the scalar field is placed at grid points and the gauge field is placed at links between two grid points. Discretized covariant derivative is defined so as to satisfy the exact gauge invariance (up to

the machine precision) while it coincides with the continuous one within the second order accuracy with respect to the lattice spacing. Field values are updated following Eqs. (4),(5) by using the Leap-frog method, satisfying the constraint equation (6) at each step.

As the initial condition, we set the random value for the phase component of the complex scalar field with the uniform probability density but the radial component is fixed to be $|\Phi| = v$ everywhere. Initial random fields are generated in the Fourier space with the cutoff scale $k_c/a = H$, above which we set zero for the field value. The time derivative of the scalar field and each component of the gauge field is initially set to be zero. Regarding the identification of cosmic string in the lattice space, we follow the method in [84] using the gauge-invariant sum of phase differences.

In order to evaluate the scaling behavior of the network of cosmic strings, we introduce two quantities. One is a mean separation between neighboring cosmic strings which is conventionally adopted in the context of the Abelian-Higgs string simulation. It has a dimension of length and defined by

$$d_{\text{sep}} = \sqrt{\frac{V_{\text{box}}}{\ell_{\text{tot}}}}, \quad (7)$$

where V_{box} is the physical volume of the simulation box and ℓ_{tot} is the total physical length of cosmic strings. When the string network follows the scaling regime, one can express it as $m_r d_{\text{sep}} = a m_r \tau + b$ with a and b being some numerical constants and $m_r \equiv \sqrt{\lambda/2}v$. The other is defined by the ratio of the string length to the Hubble length in one Hubble volume of the universe, which is conventionally used in the axion string simulation. It is dimensionless quantity defined by

$$\xi = \frac{\ell_{\text{tot}} t^2}{V_{\text{box}}}, \quad (8)$$

with t the cosmic time. In this case, $\xi = \mathcal{O}(1)$ (constant) when the string network follows the scaling regime.

In our numerical simulations, we set the grid number $N^3 = 1024^3$ and lattice spacing $\Delta x = 1/16$ (“physical” string case) or $1/2$ (“fat” string case) and start the simulation with $m_r \tau = 1$. In addition to the physical string case with λ and e being constant with time, we also consider the “fat” string case where λ and e are replaced by the time-dependent quantities, $\lambda a(t)^{-2}$ and $e a(t)^{-1}$ respectively, in order to keep the string core size and the vector core size larger than the spatial resolution of the lattice simulation. Fig. 1 shows the time evolution of the mean string separation, d_{sep} , for physical (left) and fat (right) string cases. One can see that the red lines corresponding to $e = 1$ follows the linear fitting lines $0.285 m_r \tau + 4.75$ (left) and $0.28 m_r \tau + 12.5$ (right) which are consistent with current simulations [83]. In the case with light vector boson, i.e. $e = 0.01$, the mean separation deviates from the linear fitting. It can be understood by the scaling violation as in the case with global (axion) strings. Namely, the mean separation decreases with respect to the linear fitting around the end time of the simulation, which means that the average string length becomes longer than that in the scaling regime.

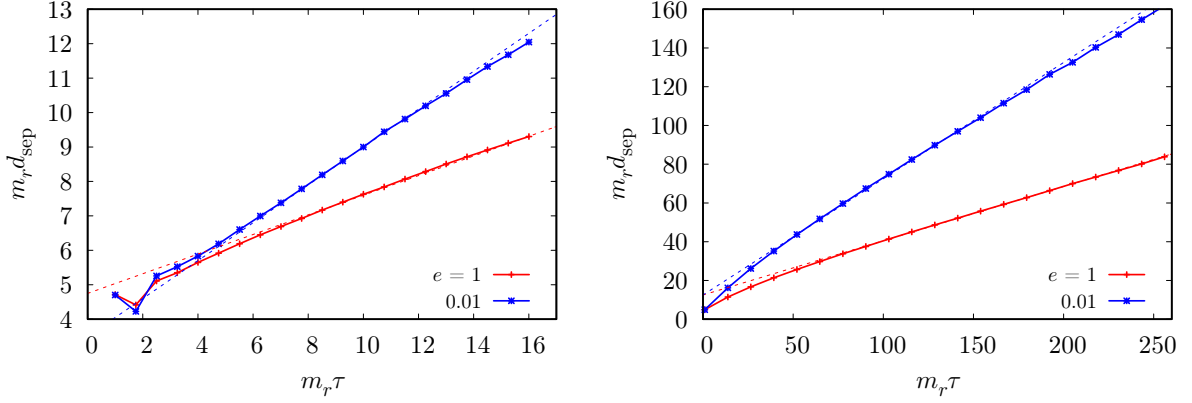


Figure 1: Time evolution of the mean separation of cosmic strings for physical (left) and fat (right) string cases. The red and blue lines correspond to $e = 1$ and $e = 0.01$ respectively. Data points are fitted by linear functions shown by thin dashed lines.

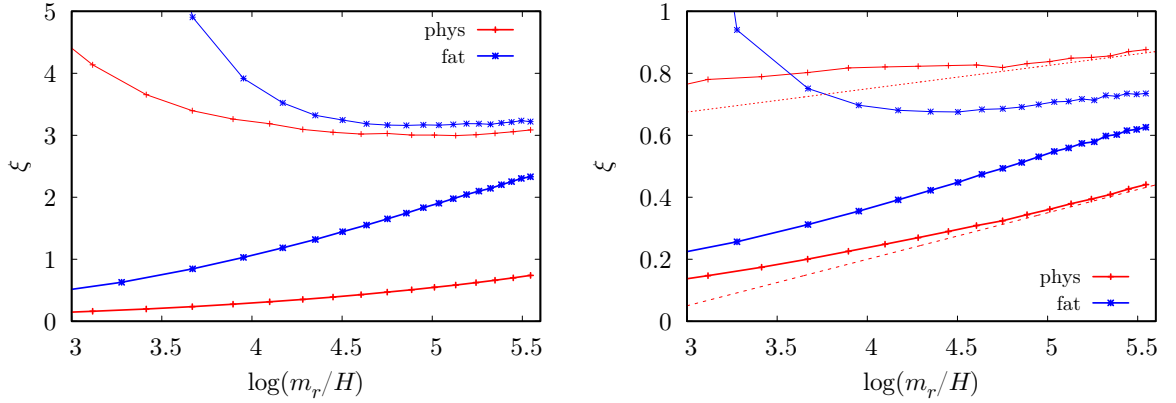


Figure 2: Time evolution of ξ for the physical (red) and fat (blue) strings with $e = 1$ (left) and $e = 0.01$ (right). Thin lines correspond to the corrected values using $\tilde{\ell}_{\text{tot}}$. In the right panel, data points with physical string cases are fitted by log functions shown by thin dotted and dashed lines.

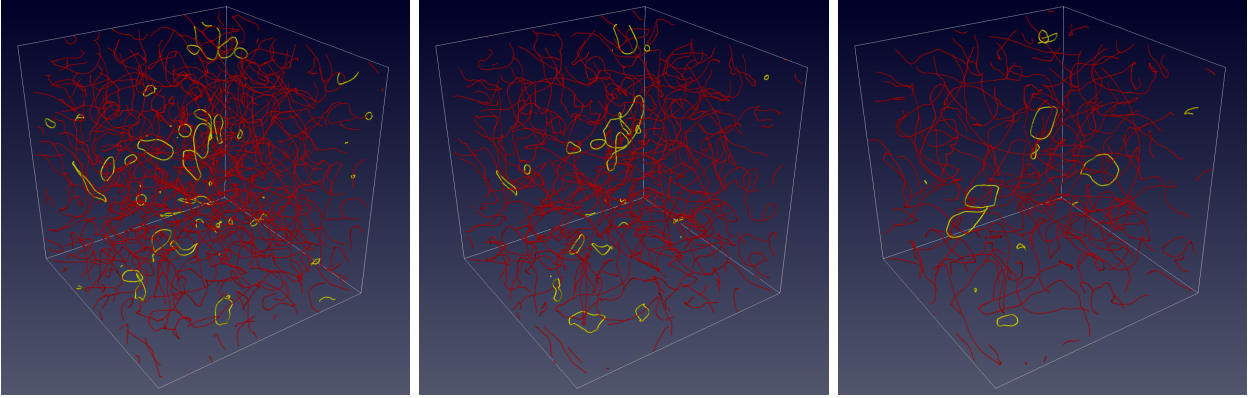


Figure 3: Snapshots of the simulation for $\lambda = 2$, $e = 1$ and $\log(m_r/H) = 3.4, 4.6, 5.3$ from left to right. Loops with comoving radius smaller than $L_{\text{box}}/(2\pi)$ are highlighted.

Fig. 2 shows time evolution of ξ . Because of the constant shift from the linear function in d_{sep} (b in the above expression), ξ cannot settle down to a constant value even in the local string case, at least in our limited simulation time. Then, we propose corrected values of d_{sep} and ℓ_{tot} so as to remove the constant shift, b , defined by

$$\tilde{d}_{\text{sep}} = \sqrt{\frac{V_{\text{box}}}{\tilde{\ell}_{\text{tot}}}} = a\tau \quad \text{with} \quad \tilde{\ell}_{\text{tot}} = \frac{V_{\text{box}}}{(\sqrt{V_{\text{box}}/\ell_{\text{tot}}} - b)^2} \quad (9)$$

One obtains the corrected value of ξ by replacing ℓ_{tot} with the corrected one. As shown in the left panel in Fig. 2 corresponding to the local string case, corrected values of ξ (thin lines) tend to be constant while original values increases with time. In the right panel, on the other hand, corrected values increases even near the end of simulation, which would be due to the scaling violation. Specifically, ξ in the right panel follows logarithmic function, $\xi = \alpha \log(m_r/H) + \beta$ with $\alpha = 0.15$ (original value) or 0.075 (corrected value). The former is consistent with the one in the previous study focusing on the axion (global) string [40, 45].

After the Hubble parameter becomes smaller than the dark photon mass, the dark photon emission from the loop collapse is kinematically suppressed. Then, one can expect that, even in the case with $e \ll 1$, the cosmic strings behave like local strings for $m_A > H$ and the scaling violation is no longer sustained. Thus, ξ tends to be constant after that. To see this, we need more grid points for the lattice simulation to follow the string network dynamics for a longer time.

Figures 3 and 4 show snapshots of time slices with $\log(m_r/H) = 3.4, 4.6, 5.3$ from left to right for $e = 1$ and 0.01 respectively. One can see more abundant small loops in the case with $e = 0.01$ corresponding to the near-global string case especially in the late time. It is due to the efficient vector boson emission as shown below.

The loop production efficiency is quantitatively shown in Figure 5, showing the number distribution of loops with logarithmic interval of loop size (ℓ) over the Hubble length ($\ell_H = H^{-1}$). Those data are obtained from 10 independent simulations with the above set up.

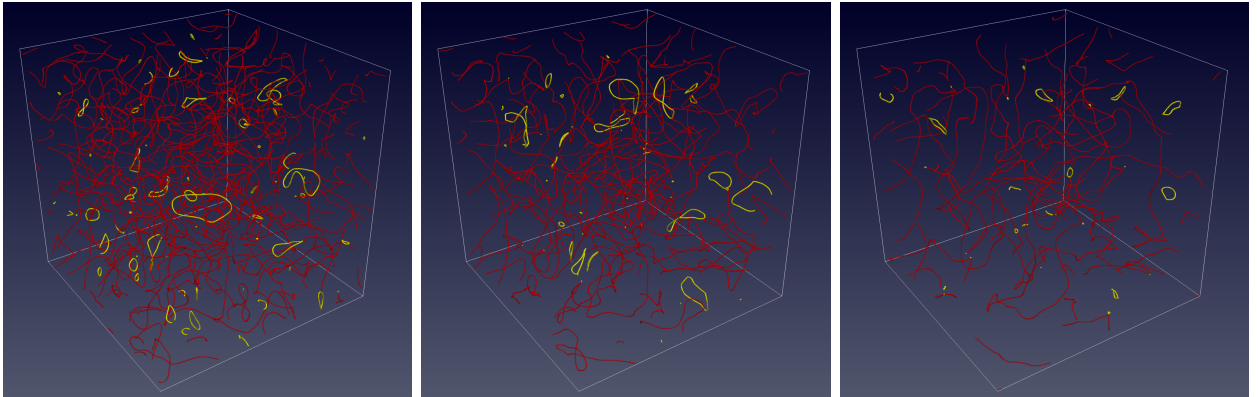


Figure 4: Same as Fig 3 but $e = 0.01$.

The vertical dotted line corresponds to $m_A \ell = 1$ and thus the loop collapse is suppressed in the right side of this line. Note that the typical initial size of the loop decoupled from the network is roughly the Hubble length, i.e. $\ell \sim \ell_H$. Hence the number of small loops cannot increase efficiently for $\ell_H > m_A^{-1}$ as one can clearly see in the local string case with $e = 1$ (top panels). This is in contrast to the near-global string case, i.e. $e = 0.01$ (bottom panels), where plenty of small loops are observed. In that case, smaller loops are more abundant because the simulation box has more Hubble patches and thus more initial Hubble-size loops are produced at earlier times. Note that total number of strings decreases with time in any case because the number of independent Hubble patches in a simulation box decreases due to the cosmic expansion.

Let us consider the dark photon emission from the network of cosmic strings. In the Abelian-Higgs model, the equivalence theorem tells us that the Nambu-Goldstone mode (i.e. the phase component) of the complex scalar field may be regarded as the longitudinal mode of the gauge field after the symmetry breaking in the relativistic limit. Thus the energy density of the longitudinal dark photon (denoted by the superscript (L)) can be obtained by the sum of the kinetic energy of the phase component of the complex scalar field and the longitudinal component of the dark electric field as follows,³

$$\rho_A^{(L)} = \frac{|\Phi|^2}{v^2} \left[\frac{2}{a^2} \left(\frac{\text{Im}(\Phi^* \Phi')}{|\Phi|} \right)^2 + \frac{1}{a^4} \left(E_i^{(L)} \right)^2 \right]. \quad (10)$$

In order to screen the cosmic string and extract only the contribution of the free dark photon, the factor $|\Phi|/v$ is multiplied as in the axion string case [40, 47]. Namely, $|\Phi|/v \simeq 0$ near the cosmic string and $|\Phi|/v = 1$ far from the string core. Note that the gradient term is highly contaminated by the cosmic string especially in the near-global string case (i.e. $e \ll 1$), so the inclusion the gradient term may cause the overestimate of the free dark photon abundance.

³Here we have imposed the gauge condition with $A_0 = 0$ (temporal gauge). Without the gauge fixing, the time derivative of Φ is replaced with the covariant derivative and thus this quantity is gauge-invariant.

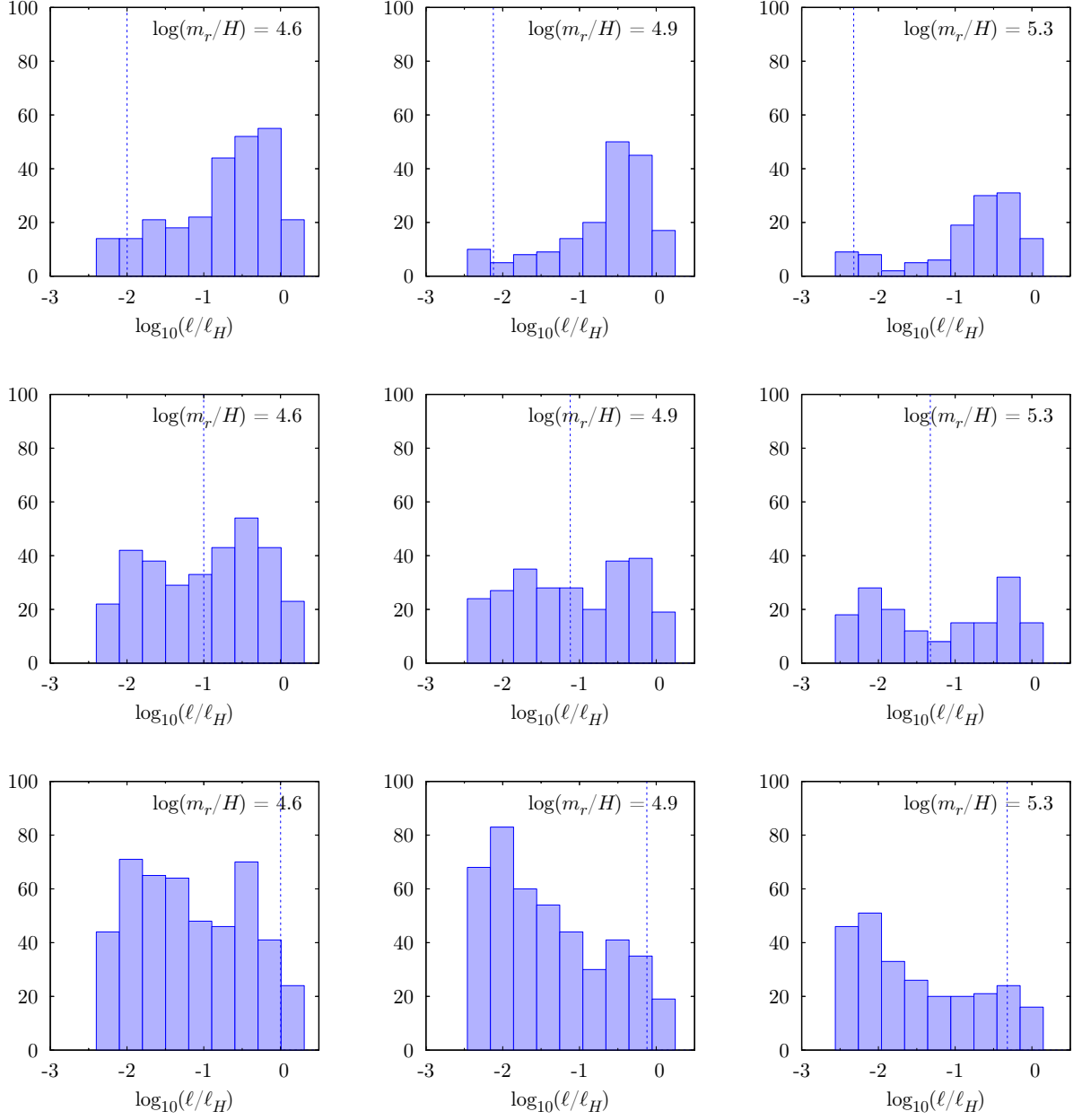


Figure 5: The number distribution of loops with respect to the loop size for $e = 1$ (top), 0.1 (middle), 0.01 (bottom). In the horizontal axis, $\ell_H \equiv H^{-1}$ is the Hubble length. Time slices correspond to $\log(m_r/H) = 4.6, 4.9, 5.3$ from left to right. The vertical dashed line corresponds to $m_A \ell = 1$.

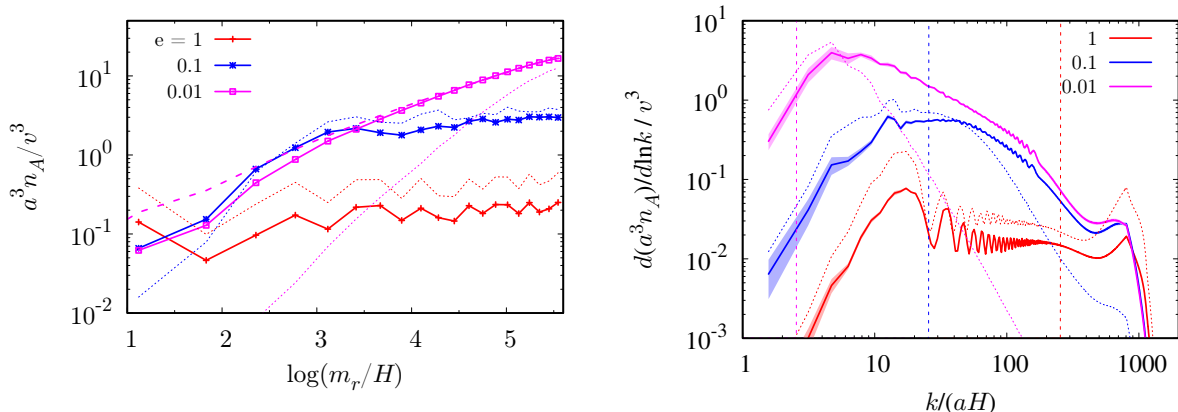


Figure 6: *Left* : Time evolution of the dark photon number density in a comoving box (left) and its spectrum at $\log(m_r/H) = 5.5$ (right) with $\lambda = 2$ ($m_r = v$), $e = 1$ (red), 0.1 (blue), 0.01 (magenta). Thick solid lines and thin dotted lines correspond respectively to the longitudinal and transverse mode. In the left figure, The magenta-dashed line represents the analytic estimation given by Eq. (12) with $\bar{E}_A/H = 10$, $\mu = \pi v^2$ and numerically obtained values of ξ . In the right panel, horizontal axis is normalized by the horizon scale and each vertical dashed line represents $k/a = m_A$.

Instead, factor 2 is multiplied in order to take into account the gradient term or mass term both of which would be comparable to the kinetic term.

To estimate the final relic abundance of the dark photon, it is convenient to calculate the number density, n_A , rather than the energy density, since n_A is conserved in a comoving volume. It can be calculated by

$$n_A = \int dk \frac{dn_A}{dk} = \int dk \frac{1}{E_A(k)} \frac{d\rho_A}{dk} \quad (11)$$

with $E_A(k) = \sqrt{(k/a)^2 + m_A^2}$. The energy spectrum $d\rho_A/dk$ can be calculated by integrating the Fourier transformation of $\text{Im}(\Phi^*\Phi')$ and $|\Phi|E_i$ with respect to the k -space solid angle. Dark photons emitted from the collapse of loops have typically Hubble-scale momenta, $k/a \sim H$. On the other hand, the emission is kinematically suppressed for $H < m_A$. Thus, a typical energy of dark photons is $E_A(k) \sim H$ at the emission. Since the energy density of emitted dark photons is proportional to that of the sting network and if the network follows the scaling law, one obtains the number density of newly produced dark photons at some cosmic time t as $\Delta n_A \sim \rho_{\text{str}}/H \propto 1/t$ and hence $a^3 \Delta n_A \propto t^{1/2}$. Therefore, such newly produced dark photons account for the dominant part of the total abundance, implying that the final dark photon abundance is determined by the number of dark photons produced at $H \sim m_A$. When the dark photons are continuously produced from the collapse of string loops, the number density of longitudinal dark photons at each time slice can be roughly estimated

as [18]

$$n_A^{(L)}(t) \simeq \frac{8\xi\mu H}{\bar{E}_A/H}, \quad (12)$$

where \bar{E}_A is the mean energy of produced dark photons.

Figure 6 shows the evolution (left) and spectrum (right) of the comoving number density of longitudinal (thick-solid lines) and transverse (thin-dotted lines) dark photons. One can see that the dark photon production is not efficient for $e = 1$. For $e = 0.1$, efficient production continues until $\log(m_r/H) \sim 3$ but it stops afterward. Persistent dark photon production has been observed for $e = 0.01$. This result can be well-fitted by Eq. (12) with $\mu = \pi v^2$ and $\bar{E}_A/H = 10$ (dashed-magenta line, which almost coincides with the data for $\log(m_r/H) \gtrsim 4$). The spectrum is mildly red-tilted ($\propto 1/k$), which explains the relative large value of \bar{E}_A/H . Note that the transverse mode is also excited around $H \sim m_A$, and thus additional two polarization modes equally contribute to the total dark photon abundance. It is equivalent to multiplying $n_A^{(L)}$ by a factor 3 to estimate the total n_A . There are several ways to understand this. In the unitary gauge, the longitudinal boson coupling is enhanced by an amount E_A/m_A due to the kinetic term normalization compared with the transverse one, whose coupling is just given by e . When $E_A \sim H \sim m_A$, they are comparable. In the Goldstone picture, the Goldstone mode θ couples like $\sim (\partial_\mu \theta/v) j^\mu$ while the transverse mode couples like $\sim e A_\mu^{(T)} j^\mu$ where $j_\mu = 2 \text{Im}(\Phi^* \partial_\mu \Phi)$ is the U(1) current which only exists at the string core. Thus it is seen that the effective Goldstone coupling is $E_A/(ev) \sim E_A/m_A$ times that of the transverse mode.⁴ Therefore, the production of transverse vector boson is inefficient at early epoch, but eventually it is comparable to the longitudinal one.

After the production stops, the number density of dark photons divided by the entropy density, n_A/s , is conserved if there is not any additional entropy production in the subsequent cosmological history. Then, one can obtain the final abundance of the dark photon

$$\Omega_A h^2 = \frac{m_A(n_{A,0}/s_0)h^2}{\rho_{\text{cr},0}/s_0} \simeq 0.091 \left(\frac{\xi}{12} \right) \left(\frac{m_A}{10^{-13} \text{ eV}} \right)^{1/2} \left(\frac{v}{10^{14} \text{ GeV}} \right)^2, \quad (13)$$

where we have substituted $\bar{E}_A/H = 10$ obtained from the simulation (see Fig. 6) and ξ is based on the following fitting formula supported by the simulation,

$$\xi = 0.15 \log \left(\frac{m_r}{m_A} \right) \simeq 12 + 0.15 \log \left[\left(\frac{m_r}{10^{14} \text{ GeV}} \right) \left(\frac{10^{-13} \text{ eV}}{m_A} \right) \right], \quad (14)$$

which is also consistent with the results of the simulation for the global strings performed in Refs. [40, 45]. Our simulation is performed with only a limited time range. To determine

⁴As a result, the relative emission rate of GWs, longitudinal vector bosons and transverse vector bosons from the string loops is estimated as $P_{\text{GW}} : P_L : P_T \sim G\mu : 1 : m_A^2/H^2$ for the string loop size $\ell \sim H^{-1} < m_A^{-1}$, where G denotes the Newton constant. In the opposite case $\ell > m_A^{-1}$ we just assume that loops cannot emit a vector boson. See next section for estimation of the GW spectrum.

more precise values of the final dark photon DM abundance, we need more refined numerical simulations using more grid points. It is left for future work.

As a remark, we assumed the radiation-dominated Universe around $H = m_A$ in deriving Eq. (13). If the reheating temperature T_R is low enough, i.e. $T_R \lesssim \sqrt{m_A M_{\text{Pl}}}$ with M_{Pl} being the reduced Planck scale, the Universe might be inflaton oscillation dominated at $H = m_A$. In such a case, assuming that the inflaton oscillation behaves as non-relativistic matter, the final abundance should be multiplied by a factor $T_R/\sqrt{m_A M_{\text{Pl}}}$ to Eq. (13), up to some corrections to numerical factor, which indicates that the abundance becomes independent of m_A .

3 Gravitational wave background from cosmic strings

In this section we derive the spectrum of stochastic GW background from cosmic strings. In the dark photon DM scenario, a big difference from the case of local strings and pure global strings is that the dark photon is very light but still massive. The short loops that are created in the early Universe promptly decay through the dark photon emission and hence the GW emission efficiency is suppressed, while long loops that are created in relatively recent epoch cannot lose their energy through the dark photon emission. Thus the resulting GW spectrum will be significantly different from both the (pure) local string and global case.

3.1 Energy loss of loops

The energy density of the cosmic string network in the scaling regime is

$$\rho_{\text{str}}(t) = \xi(t) \frac{\mu(t)}{t^2}, \quad (15)$$

where the ξ parameter is given by (14). The string tension may be given by $\mu = 2\pi v^2 \log(m_r/H)$ for the global string case. Within Hubble time, cosmic strings intersect with each other, forming loops which eventually decays emitting GWs or light vector bosons. The energy loss rate of a loop is given by

$$\frac{dE_\ell}{dt} = -\Gamma_{\text{GW}} G \mu^2 - \Gamma_{\text{vec}} v^2 \theta(1 - m_A \ell), \quad (16)$$

where $\Gamma_{\text{GW}} \sim \Gamma_{\text{vec}} \sim 50$ are numerical constants. The step function ensures that the loop cannot emit vector boson if the inverse loop size is smaller than the vector boson mass. For small loops $m_A \ell_i < 1$, the loop length at the time t with an initial length ℓ_i is given by

$$\ell(t) = \ell_i - \Gamma_{\text{eff}}(t - t_i), \quad (17)$$

where

$$\Gamma_{\text{eff}} \equiv \Gamma_{\text{GW}} G \mu + \frac{\Gamma_{\text{vec}}}{\pi \log(m_r/H_i)}. \quad (18)$$

For estimating the loop lifetime, the GW contribution is negligible unless the symmetry breaking v is very close to the Planck scale. Thus the loop lifetime is

$$\tau(\ell_i) \simeq \frac{\pi \log(m_r/H_i)}{\Gamma_{\text{vec}}} \ell_i. \quad (19)$$

Up to a numerical factor of $\mathcal{O}(1)$, $\tau(\ell_i) \sim \ell_i$ in this case. Since $\ell_i < t_i$, the lifetime is shorter than the Hubble time. On the other hand, for large loops $m_A \ell_i > 1$, the GW emission is the only energy loss process⁵ and we have

$$\tau(\ell_i) \simeq \frac{\ell_i}{\Gamma_{\text{GW}} G \mu}. \quad (20)$$

Thus, for $\ell_i > \Gamma_{\text{GW}} G \mu t_i$, the loops are long-lived, i.e., the lifetime is longer than the Hubble time.

3.2 Loop density

To maintain the scaling solution (15), the infinite strings cast their energy into string loops. An energy fraction $C_{\text{loop}} \sim 10\%$ of the total string energy density is considered to go into the loops within one Hubble time. The loops lose their energy due to the emission of vector bosons or GWs. As far as $v \ll M_{\text{Pl}}$ and the vector boson is much lighter than the inverse loop size $m_A \lesssim \ell^{-1}$, the emission of (longitudinal) vector boson is much more efficient than that into GWs. Even the Hubble-size loops decay within one Hubble time by the emission of vector bosons. Still, a small fraction of loop energy goes into GWs and also notice that loops larger than the inverse vector boson mass cannot emit vector boson and hence GW emission is the dominant source of the energy loss. Below we estimate the stochastic GW background spectrum generated from the string loop decays.⁶

Let us denote the number density of string loops with a loop length ℓ per logarithmic bin of ℓ produced at the cosmic time t as $[dn_\ell/d \ln \ell(t)]_{\text{prod}}$. The total energy density of the string loops, averaged over the Hubble time, is

$$\rho_{\text{loop}}(t) = \int \frac{t + \tau(\ell)}{\tau(\ell)} \left[\frac{d\rho_\ell(t)}{d \ln \ell} \right]_{\text{prod}} d \ln \ell = \int \mu \ell \frac{t + \tau(\ell)}{\tau(\ell)} \left[\frac{dn_\ell(t)}{d \ln \ell} \right]_{\text{prod}} d \ln \ell, \quad (21)$$

where the subscript “prod” indicates the energy/number density of loops that are produced at the time t with the Hubble time interval and the factor $\frac{t+\tau(\ell)}{\tau(\ell)}$ is introduced taking account of the finite lifetime of the loop. If the loop lifetime $\tau(\ell)$ is shorter than the Hubble time t , loops exist only in a short fractional time interval $\tau(\ell)/t$ within one Hubble time.

The loops have some distributions on the initial loop length ℓ_i . There are several studies on the initial loop size, but no definite conclusions have not been reached yet. Our simulation

⁵Still it can emit vector bosons from small scale irregularities on the loops. We do not consider it in this paper.

⁶GWs are also produced from infinite strings [85–87], which we will not pursue in this paper.

in Sec. 2 is also not enough to determine the loop distribution for very late Universe due to the limited dynamical range of the simulation. Instead, we consider typical possibilities for the initial distribution of α . One is the monochromatic distribution,

$$\left[\frac{dn_\ell(t)}{d \ln \ell} \right]_{\text{prod}} = \frac{\tau(\ell)}{t + \tau(\ell)} \frac{C_{\text{loop}} \xi}{\alpha_0 t^3} \ell \delta(\ell - \alpha_0 t), \quad (22)$$

where $\alpha_0 = 0.1$ will be taken. The overall normalization is determined such that $\rho_{\text{loop}}(t) = C_{\text{loop}} \rho_{\text{str}}(t)$. The other is the flat distribution in the log spacing of ℓ in the interval $m_r^{-1} < \ell < \alpha_0 t$ [40] (which we call “log-flat distribution”),

$$\left[\frac{dn_\ell(t)}{d \ln \ell} \right]_{\text{prod}} = [\alpha_0 + \Gamma_{\text{eff}} \log(\alpha_0 t m_r)]^{-1} \frac{C_{\text{loop}} \xi}{t^3} \Theta(\ell; m_r^{-1}, \alpha_0 t) \quad (23)$$

where the function $\Theta(t; x, y)$ is defined as

$$\Theta(t; x, y) = \begin{cases} 1 & \text{for } x < t < y \\ 0 & \text{otherwise} \end{cases}. \quad (24)$$

Again, the overall normalization is determined such that $\rho_{\text{loop}}(t) = C_{\text{loop}} \rho_{\text{str}}(t)$. If the vector boson emission is efficient we have $\tau(\ell) \sim \ell$ and if it is kinematically suppressed, the GW emission is dominant and we have $\tau(\ell) \gg \ell$. Thus the numerical factor in the parenthesis is always $\mathcal{O}(1)$.

After the formation of loops at $t = t_i$, their number density decrease as $a(t)^{-3}$ until they decay at $t = t_i + \tau(\ell)$. Thus the number density of loops of length ℓ measured at t that were produced at $t = t_i$ is

$$\frac{dn_\ell(t; t_i)}{d \ln \ell} = \left[\frac{dn_\ell(t_i)}{d \ln \ell_i} \right]_{\text{prod}} \left(\frac{a(t_i)}{a(t)} \right)^3 \theta(t - t_i), \quad (25)$$

where the initial loop size ℓ_i will evolve according to (17). The total loop number density of length ℓ at the time t is then given by the integration over the production time t_i :

$$\frac{dn_\ell(t)}{d \ln \ell} = \int^t d \ln t_i \frac{dn_\ell(t; t_i)}{d \ln \ell_i}. \quad (26)$$

For the case of monochromatic distribution (22), the loop length ℓ_i and the production time t_i has one-to-one correspondence as $\ell_i = \alpha_0 t_i$. We obtain

$$\frac{dn_\ell(t)}{d \ln \ell} \simeq \frac{\tau(\ell)}{\tau(\ell) + t_i} \frac{C_{\text{loop}} \xi(t_i)}{\alpha_0 t_i^3} \left(\frac{a(t_i)}{a(t)} \right)^3 \theta \left(t - \frac{\ell_i}{\alpha_0} \right), \quad (27)$$

where

$$t_i = \frac{\ell + \Gamma_{\text{eff}} t}{\alpha_0 + \Gamma_{\text{eff}}}. \quad (28)$$

For the case of log-flat distribution (23), by noting that the integral over t_i is dominated by the lower edge $t_i \simeq \ell_i/\alpha_0$, we obtain

$$\frac{dn_\ell(t)}{d \ln \ell} \simeq \frac{1}{\alpha_0 + \Gamma_{\text{eff}} \log(\alpha_0 t m_\tau)} \frac{C_{\text{loop}} \xi(t_i)}{t_i^3} \left(\frac{a(t_i)}{a(t)} \right)^3 \theta \left(t - \frac{\ell_i}{\alpha_0} \right). \quad (29)$$

By noting that the factor $\frac{\tau(\ell)}{\tau(\ell)+t_i}$ is at least $\mathcal{O}(0.1)$ in the monochromatic distribution with $\alpha_0 \sim \mathcal{O}(0.1)$, we can see that the monochromatic and log-flat distributions do not give much differences for the purpose of orders-of-magnitude estimation. Below we use the monochromatic distribution for simplicity.

3.3 Gravitational wave spectrum

The GW power radiated from each loop with the size ℓ into the GW frequency f is given by

$$\frac{dP_{\text{GW}}(\ell)}{d \ln f} = G\mu^2 f \ell S(f\ell), \quad (30)$$

where the spectral function $S(x)$ takes the form

$$S(x) = (q-1)2^{q-1}\Gamma_{\text{GW}} \frac{\theta(x-2)}{x^q}, \quad (31)$$

where $q > 1$ is assumed and the overall normalization is determined so that $\int dx S(x) = \Gamma_{\text{GW}} \sim 50$. The slope q depends on the origin: for cusps on the loop $S(x) \propto x^{-4/3}$ [49] and for kinks $S(x) \propto x^{-5/3}$ [50, 54, 58]. Since the cusp contribution is dominant, we take $q = 4/3$ in the following.

The GW energy density with the frequency between $[f, f + df]$ produced by the loops with length between $[\ell, \ell + d\ell]$ per unit time at the time t is given by

$$\frac{d\rho_{\text{GW}}(t)}{dt} = \frac{dP_{\text{GW}}(\ell)}{df} \times \frac{dn_\ell(t)}{d\ell} d\ell \times df(t). \quad (32)$$

The present GW frequency f_0 is given by $f_0 = f(t)a(t)/a_0$ and the energy density scales as $\rho_{\text{GW}} \propto a^{-4}$. Thus the present GW spectrum is expressed as⁷

$$\frac{d\rho_{\text{GW}}(t_0)}{df_0} = \int dt \int d\ell G\mu^2(t) S \left(\frac{\ell f_0 a_0}{a(t)} \right) \frac{dn_\ell(t)}{d \ln \ell} \left(\frac{a(t)}{a_0} \right)^3. \quad (33)$$

It is convenient to express it in terms of the density parameter

$$\Omega_{\text{GW}}(f_0) = \frac{1}{\rho_{\text{crit}}} \frac{d\rho_{\text{GW}}(t_0)}{d \ln f_0}. \quad (34)$$

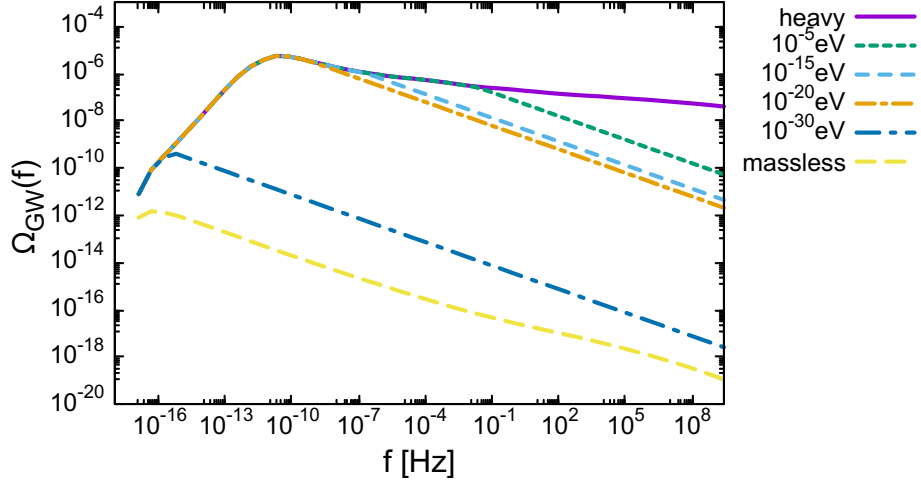
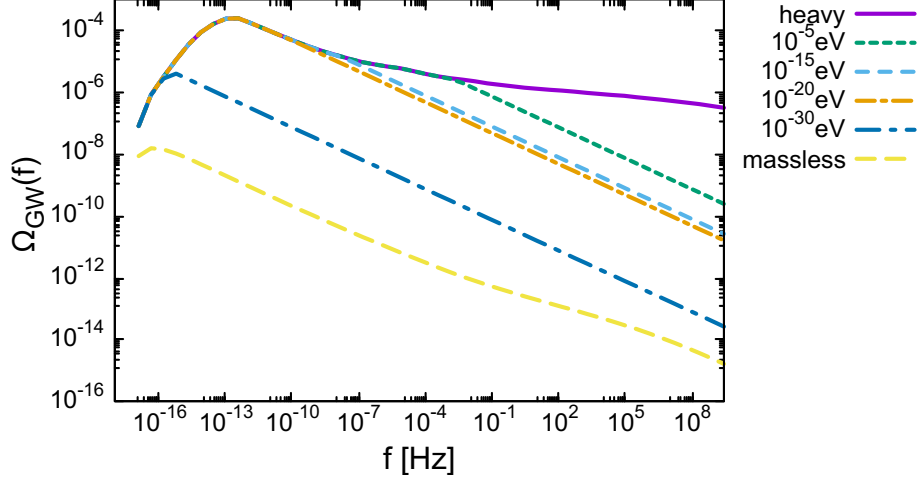


Figure 7: The present day gravitational wave spectrum for $m_A = (\infty, 10^{-5}, 10^{-15}, 10^{-20}, 10^{-30}, 0)$ eV, respectively. We have taken $v = 10^{15}$ GeV in the top panel and $v = 10^{14}$ GeV in the bottom panel.

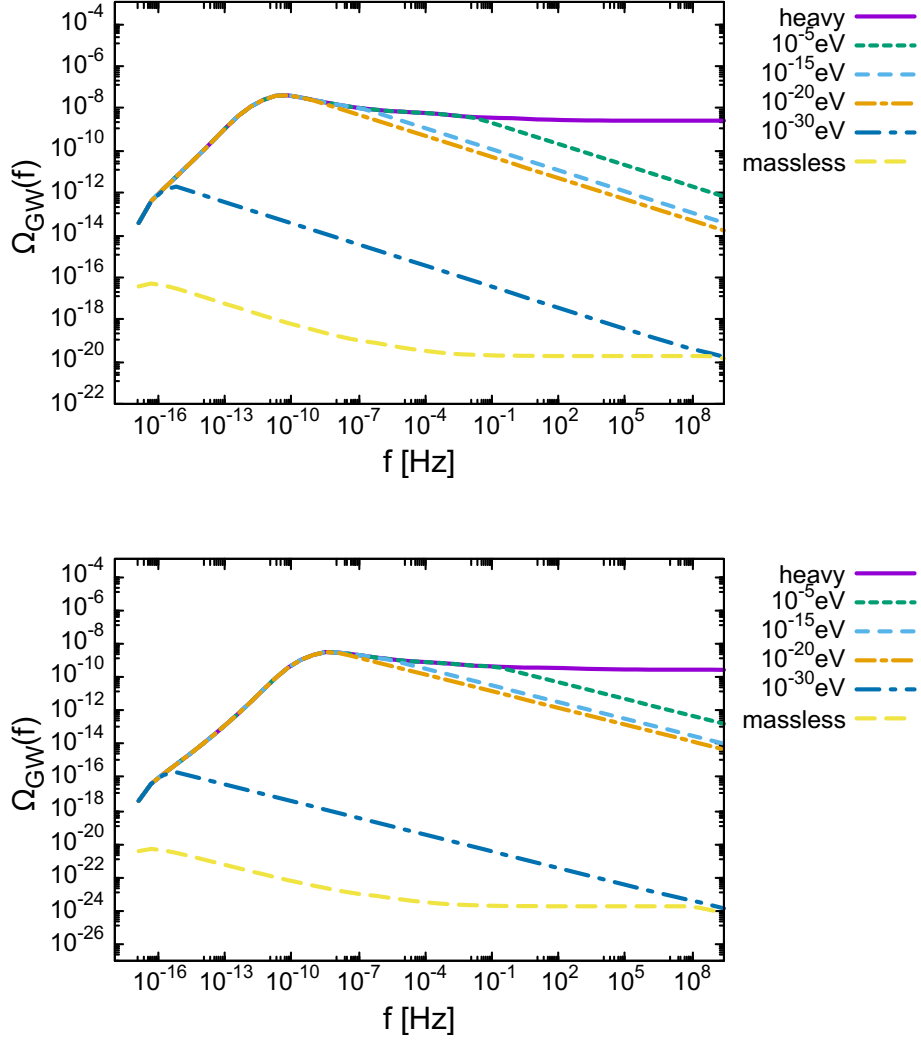


Figure 8: The present day gravitational wave spectrum for $m_A = (\infty, 10^{-5}, 10^{-15}, 10^{-20}, 10^{-30}, 0)$ eV, respectively. We have taken $v = 10^{15}$ GeV in the top panel and $v = 10^{14}$ GeV in the bottom panel. We have neglected all the log dependence by hand for illustrative purpose.

Fig. 7 shows the present day gravitational wave spectrum for $m_A = (\infty, 10^{-5}, 10^{-15}, 10^{-20}, 10^{-30}, 0)$ eV respectively. We have taken $v = 10^{15}$ GeV in the top panel and $v = 10^{14}$ GeV in the bottom panel. For reference, $v = 10^{15}$ (10^{14}) GeV corresponds to $G\mu = 4 \times 10^{-8}$ (4×10^{-10}) in terms of the frequently used parametrization $G\mu$ for the case of local string. We have assumed monochromatic distribution for the loops. For illustrative purpose, we also show the spectrum with neglecting the log dependence by hand (i.e. $\xi = 0.15$ and $\mu = 2\pi v^2$) in Fig. 8. We have used the fitting formula given in Ref. [88] for the relativistic degrees of freedom g_* and g_{*s} for arbitrary redshift.

Let us explain a bit more detail. First let us see Fig. 8 where the log dependence is dropped by hand.

- The case without vector boson emission (“heavy” line in Fig. 8) is just the same as the local string case. The flat part is roughly given by $\sim \sqrt{G\mu}\Omega_{\text{rad}}$, since the fraction of loop energy density, which was created at $t = t_i$, to the total energy density is $\sim G\mu \times [a(\tau(\ell))/a(t_i)] \sim \sqrt{G\mu}$ when the loop decays at $t = \tau(\ell)$ and all the energy of loops go to the GW emission.⁸ The low frequency limit of the GW spectrum is dominated by the loops with lifetime longer than the present age of the Universe, which emit GWs around $z \sim 1$. If $\alpha t_{\text{eq}} < \Gamma_{\text{GW}} G\mu t_0$, with t_{eq} being the cosmic time at the matter-radiation equality, all the loops that are created at the radiation dominated era completely decays until the present age. In this case, the low frequency spectrum is determined by the loops that are created at the matter domination era and it behaves as $\Omega_{\text{GW}} \propto f$. In the opposite case, $\alpha t_{\text{eq}} > \Gamma_{\text{GW}} G\mu t_0$, loops that are created in the radiation dominated era can also exist in the present Universe and it gives a contribution like $\Omega_{\text{GW}} \propto f^{3/2}$. For even lower frequency, loops that are created in the matter-dominated era contributes, which behaves as $\Omega_{\text{GW}} \propto f$. The peak of the spectrum corresponds to GWs from loops that are decaying in the present Universe. Such loops produce $f^{-1/3}$ tail towards higher frequency part until it crosses the flat part mentioned above. The peak frequency is roughly given by $f \sim (\Gamma_{\text{GW}} G\mu t_0)^{-1}$ and the peak spectrum is given by $\Omega_{\text{GW}} \sim G\mu$ for $\alpha t_{\text{eq}} < \Gamma_{\text{GW}} G\mu t_0$ and $\Omega_{\text{GW}} \sim \sqrt{G\mu\alpha/\Gamma_{\text{GW}}}\Omega_{\text{rad}}^{3/4}$ for $\alpha t_{\text{eq}} > \Gamma_{\text{GW}} G\mu t_0$.
- On the other hand, for the massless limit (“massless” line in Fig. 8), the string loops are short-lived, i.e., they decay within one Hubble time. The overall normalization of the GW spectrum at the flat part is given by $\sim (G\mu)^2\Omega_{\text{rad}}$, since the most energy is consumed by the vector boson emission and only the small fraction $\sim G\mu$ of each loop goes to the GW emission. The lower frequency part is proportional to $f^{-1/3}$, which is a tail of the spectrum (31) sourced by the loops of the size $\sim \alpha_0 t_0$, which are produced around $z \sim 1$.

⁷To be precise, one may subtract GWs from “rare burst” events at relatively low redshift for estimating the stochastic GW background [53, 54].

⁸Here we assumed that the loop was created and decays in the radiation dominated era. Note also that for very high frequency beyond the loop size that is created at the epoch of phase transition, the GW spectrum decreases as $f^{-1/3}$, which comes from the tail of the spectrum (31).

- By assuming finite vector boson mass m_A , there appear a break in the GW spectrum. For larger loops that are produced at later epochs the vector boson emission is prohibited and hence the GW spectrum in the low-frequency limit is similar to those in the massive limit. On the other hand, for smaller loops the GW emission is strongly suppressed because of the vector boson emission. Thus the high frequency part is dominated by the $f^{-1/3}$ tail of the GW emission from large loops as described by the function (31). Practically, small loops that are created in earlier epoch of the Universe decay into vector bosons and do not contribute to the present GW spectrum. It is hidden by the $f^{-1/3}$ tail coming from large long-lived loops that are decaying around $z \sim 1$.
- The overall picture is similar for the case including the log dependence (Fig. 7). Due to the log enhancement, the overall spectrum tilt is seen and the overall normalization also becomes significantly larger than the case without log dependence, since the string tension μ and ξ parameter gets a log enhancement factor that directly increases the GW amplitude. The “massless” line of Fig. 7 is consistent with that given in Ref. [66], where the case of global strings with massless axion has been analyzed.

In Fig. 9 the calculated GW spectrum is compared with current and future sensitivities of various experiments: ground-based GW detectors such as LIGO [89,90], VIRGO [91], Einstein Telescope (ET) [92], space laser interferometers such as LISA [93], DECIGO/BBO [94], and pulsar timing arrays such as European Pulsar Timing Array (EPTA) [95], NANOGrav [96], Square Kilometer Array (SKA) [97]. The sensitivity lines are taken from Refs. [98,99]. Note that lines of SKA, LISA, DECIGO/BBO and ET represent future sensitivities and others correspond to already existing bounds. We show three lines corresponding to benchmark points in which correct dark photon DM abundance is obtained within an order of magnitude (see Eq. (13)): (a) $(v, m_A) = (10^{14} \text{ GeV}, 10^{-13} \text{ eV})$, (b) $(10^{13} \text{ GeV}, 10^{-9} \text{ eV})$, (c) $(10^{12} \text{ GeV}, 10^{-4} \text{ eV})$.

An interesting feature seen in Fig. 9 is that the three lines (a)-(c) converge in high-frequency limit. It is understood as follows. As explained above, the overall normalization of the GW spectrum is proportional to $\sqrt{G\mu}$ for long-lived loops. The spectral break appears at the frequency f_{break} that corresponds to the inverse of the loop size $\ell_i = \alpha_0 t_i \sim m_A^{-1}$, which decays at $\tau(\ell_i) \sim \ell_i / (\Gamma_{\text{GW}} G \mu)$. The GW spectrum behaves as $\Omega_{\text{GW}} \propto f^{-1/3}$ for $f > f_{\text{break}}$. The break frequency is estimated as $f_{\text{break}} \sim \ell_i^{-1} [a(\tau(\ell_i)) / a_0] \propto \sqrt{m_A / \mu}$ assuming that the corresponding loops are produced in the radiation-dominated era. On the other hand, the dark photon DM abundance is proportional to the combination $\mu \sqrt{m_A}$ (see Eq. (13)). By requiring the consistent dark photon DM abundance, we obtain $f_{\text{break}} \propto \mu^{-3/2}$. Therefore, we have $\Omega_{\text{GW}}(f_{\text{break}}) \propto f_{\text{break}}^{-1/3}$. This power law dependence coincides with the $f^{-1/3}$ tail (31). This is the reason why three lines (a)-(c) converge. It means that the GW amplitude at high frequency (e.g. in the DECIGO/BBO frequency range) is nearly independent of the dark photon mass if its abundance is consistent with the observed DM abundance. The parameter degeneracy is solved by combining with the low frequency observation, e.g. by SKA.

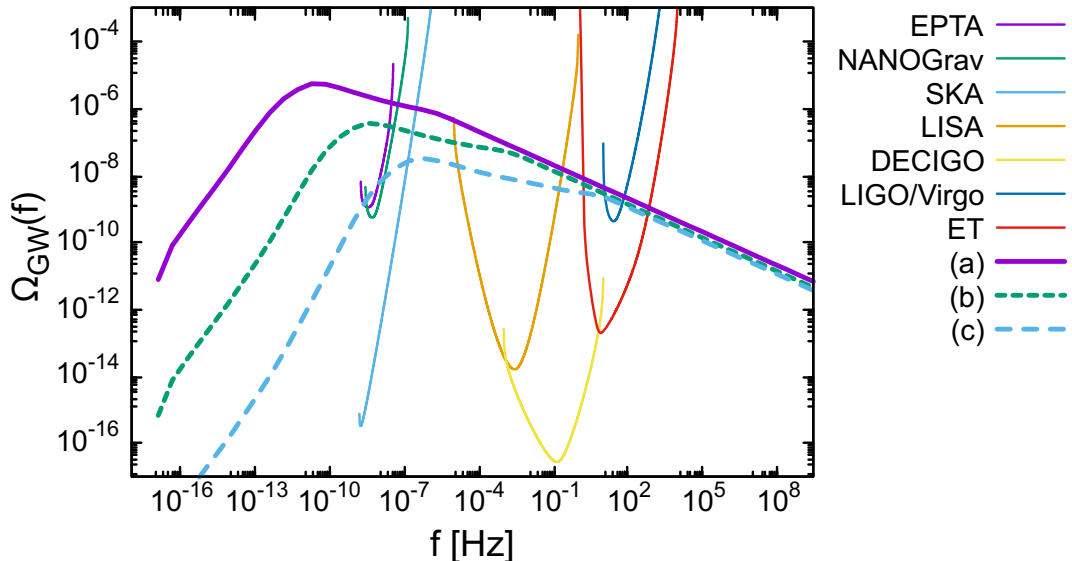


Figure 9: GW spectrum from cosmic strings in the dark photon DM scenario, compared with current and future sensitivities of various experiments. Three theoretical lines correspond to benchmark points in which correct dark photon DM abundance is obtained: (a) $(v, m_A) = (10^{14} \text{ GeV}, 10^{-13} \text{ eV})$, (b) $(10^{13} \text{ GeV}, 10^{-9} \text{ eV})$, (c) $(10^{12} \text{ GeV}, 10^{-4} \text{ eV})$.

It is seen that $v \gg 10^{12} \text{ GeV}$ or $m_A \ll 10^{-5} \text{ eV}$ is already excluded by the pulsar timing constraints. Also it should be noticed that the on-going ground-based experiments, LIGO/Virgo, may be able to detect GWs independently of the dark photon mass. However, one should note that there may be several orders-of-magnitude uncertainties on the GW spectrum, especially from the log dependence of the string tension and ξ parameter and also the loop abundance and such uncertainties significantly affect the resulting constraint on the symmetry breaking scale v and the dark photon mass m_A . For example, if the GW spectrum is reduced by one order of magnitude due to these uncertainties, $m_A \sim 10^{-10}$ may be allowed. Thus we need more accurate theoretical calculations to derive precise constraint. In any case, future space laser-interferometers such as LISA and DECIGO/BBO, ground-based detectors such as ET and also the radio wave observations of pulsars by SKA have good chances to detect GWs from cosmic strings in the dark photon DM scenario.

4 Conclusions and discussion

We found that the dark photon DM scenario from cosmic strings predict sizable amount of stochastic GW background, which may already be excluded by pulsar timing observations for $v \gg 10^{12} \text{ GeV}$ or $m_A \ll 10^{-5} \text{ eV}$. The constraint on the string tension is stronger than the conventional local string case due to the logarithmic enhancement of the string tension and ξ parameter. However, we need more precise study on this issue considering the large

scale separation between v and m_A or the Hubble parameter, which is far beyond the reach of numerical simulation, since $\mathcal{O}(10)$ change in the GW spectrum would lead to orders-of-magnitude change to the constraint on v or m_A .

Some notes are in order. In calculating the GW spectrum, we made a simple assumption that loops longer than the inverse vector boson mass m_A^{-1} cannot emit vector bosons. It may be a too simplified assumption since small scale irregularities may be present on long loops that allow to emit vector boson and long loops may lose their energy through the vector boson emission. Still we expect that the overall picture does not change drastically, since the energy of the order of $\mu\ell$ remains for the loop length ℓ even if such irregularities are smoothed out by the vector boson emission, and eventually it should be compensated by the GW emission. Another general remark is that the $f^{-1/3}$ tail of the GW spectrum represented by (31) is quite important in broad frequency range as seen in figures. This power law behavior assumes that the cusp on the loop dominates the GW emission. While it is natural to consider that cusps take important roles since cusps are necessarily formed periodically on the string loop according to the Nambu-Goto action [24], still it requires more investigation whether it remains true in the case of our interest. These are left for a future work.

Acknowledgment

This work was supported by JSPS KAKENHI Grant Nos. 17H06359 (K.N.), 18K03609 (K.N.), 19H01894 (N.K.), 20H01894 (N.K.), 20H05851 (N.K.), 21H01078 (N.K.), 21KK0050 (N.K.). This work was supported by World Premier International Research Center Initiative (WPI), MEXT, Japan.

References

- [1] M. Fabbrichesi, E. Gabrielli, and G. Lanfranchi, “The Dark Photon,” [arXiv:2005.01515 \[hep-ph\]](#).
- [2] A. Caputo, A. J. Millar, C. A. J. O’Hare, and E. Vitagliano, “Dark photon limits: A handbook,” *Phys. Rev. D* **104** no. 9, (2021) 095029, [arXiv:2105.04565 \[hep-ph\]](#).
- [3] M. Goodsell, J. Jaeckel, J. Redondo, and A. Ringwald, “Naturally Light Hidden Photons in LARGE Volume String Compactifications,” *JHEP* **11** (2009) 027, [arXiv:0909.0515 \[hep-ph\]](#).
- [4] M. Cicoli, M. Goodsell, J. Jaeckel, and A. Ringwald, “Testing String Vacua in the Lab: From a Hidden CMB to Dark Forces in Flux Compactifications,” *JHEP* **07** (2011) 114, [arXiv:1103.3705 \[hep-th\]](#).
- [5] P. W. Graham, J. Mardon, and S. Rajendran, “Vector Dark Matter from Inflationary Fluctuations,” *Phys. Rev. D* **93** no. 10, (2016) 103520, [arXiv:1504.02102 \[hep-ph\]](#).

- [6] Y. Ema, K. Nakayama, and Y. Tang, “Production of purely gravitational dark matter: the case of fermion and vector boson,” *JHEP* **07** (2019) 060, [arXiv:1903.10973](#) [[hep-ph](#)].
- [7] A. Ahmed, B. Grzadkowski, and A. Socha, “Gravitational production of vector dark matter,” *JHEP* **08** (2020) 059, [arXiv:2005.01766](#) [[hep-ph](#)].
- [8] E. W. Kolb and A. J. Long, “Completely dark photons from gravitational particle production during the inflationary era,” *JHEP* **03** (2021) 283, [arXiv:2009.03828](#) [[astro-ph.CO](#)].
- [9] T. Sato, F. Takahashi, and M. Yamada, “Gravitational production of dark photon dark matter with mass generated by the Higgs mechanism,” *JCAP* **08** no. 08, (2022) 022, [arXiv:2204.11896](#) [[hep-ph](#)].
- [10] M. Redi and A. Tesi, “Dark photon Dark Matter without Stueckelberg mass,” *JHEP* **10** (2022) 167, [arXiv:2204.14274](#) [[hep-ph](#)].
- [11] Y. Tang and Y.-L. Wu, “On Thermal Gravitational Contribution to Particle Production and Dark Matter,” *Phys. Lett. B* **774** (2017) 676–681, [arXiv:1708.05138](#) [[hep-ph](#)].
- [12] M. Garny, A. Palessandro, M. Sandora, and M. S. Sloth, “Theory and Phenomenology of Planckian Interacting Massive Particles as Dark Matter,” *JCAP* **02** (2018) 027, [arXiv:1709.09688](#) [[hep-ph](#)].
- [13] P. Agrawal, N. Kitajima, M. Reece, T. Sekiguchi, and F. Takahashi, “Relic Abundance of Dark Photon Dark Matter,” *Phys. Lett. B* **801** (2020) 135136, [arXiv:1810.07188](#) [[hep-ph](#)].
- [14] R. T. Co, A. Pierce, Z. Zhang, and Y. Zhao, “Dark Photon Dark Matter Produced by Axion Oscillations,” *Phys. Rev. D* **99** no. 7, (2019) 075002, [arXiv:1810.07196](#) [[hep-ph](#)].
- [15] M. Bastero-Gil, J. Santiago, L. Ubaldi, and R. Vega-Morales, “Vector dark matter production at the end of inflation,” *JCAP* **04** (2019) 015, [arXiv:1810.07208](#) [[hep-ph](#)].
- [16] J. A. Dror, K. Harigaya, and V. Narayan, “Parametric Resonance Production of Ultralight Vector Dark Matter,” *Phys. Rev. D* **99** no. 3, (2019) 035036, [arXiv:1810.07195](#) [[hep-ph](#)].
- [17] K. Nakayama and W. Yin, “Hidden photon and axion dark matter from symmetry breaking,” *JHEP* **10** (2021) 026, [arXiv:2105.14549](#) [[hep-ph](#)].

- [18] A. J. Long and L.-T. Wang, “Dark Photon Dark Matter from a Network of Cosmic Strings,” *Phys. Rev. D* **99** no. 6, (2019) 063529, [arXiv:1901.03312 \[hep-ph\]](#).
- [19] A. E. Nelson and J. Scholtz, “Dark Light, Dark Matter and the Misalignment Mechanism,” *Phys. Rev. D* **84** (2011) 103501, [arXiv:1105.2812 \[hep-ph\]](#).
- [20] P. Arias, D. Cadamuro, M. Goodsell, J. Jaeckel, J. Redondo, and A. Ringwald, “WISPy Cold Dark Matter,” *JCAP* **06** (2012) 013, [arXiv:1201.5902 \[hep-ph\]](#).
- [21] K. Nakayama, “Vector Coherent Oscillation Dark Matter,” *JCAP* **10** (2019) 019, [arXiv:1907.06243 \[hep-ph\]](#).
- [22] K. Nakayama, “Constraint on Vector Coherent Oscillation Dark Matter with Kinetic Function,” *JCAP* **08** (2020) 033, [arXiv:2004.10036 \[hep-ph\]](#).
- [23] Y. Nakai, R. Namba, and I. Obata, “Peaky Production of Light Dark Photon Dark Matter,” [arXiv:2212.11516 \[hep-ph\]](#).
- [24] A. Vilenkin and E. P. S. Shellard, *Cosmic Strings and Other Topological Defects*. Cambridge University Press, 7, 2000.
- [25] R. L. Davis, “Cosmic Axions from Cosmic Strings,” *Phys. Lett. B* **180** (1986) 225–230.
- [26] D. Harari and P. Sikivie, “On the Evolution of Global Strings in the Early Universe,” *Phys. Lett. B* **195** (1987) 361–365.
- [27] R. L. Davis and E. P. S. Shellard, “DO AXIONS NEED INFLATION?,” *Nucl. Phys. B* **324** (1989) 167–186.
- [28] A. Dabholkar and J. M. Quashnock, “Pinning Down the Axion,” *Nucl. Phys. B* **333** (1990) 815–832.
- [29] C. Hagmann and P. Sikivie, “Computer simulations of the motion and decay of global strings,” *Nucl. Phys. B* **363** (1991) 247–280.
- [30] R. A. Battye and E. P. S. Shellard, “Global string radiation,” *Nucl. Phys. B* **423** (1994) 260–304, [arXiv:astro-ph/9311017](#).
- [31] R. A. Battye and E. P. S. Shellard, “Axion string constraints,” *Phys. Rev. Lett.* **73** (1994) 2954–2957, [arXiv:astro-ph/9403018](#). [Erratum: *Phys.Rev.Lett.* 76, 2203–2204 (1996)].
- [32] M. Yamaguchi, M. Kawasaki, and J. Yokoyama, “Evolution of axionic strings and spectrum of axions radiated from them,” *Phys. Rev. Lett.* **82** (1999) 4578–4581, [arXiv:hep-ph/9811311](#).

- [33] M. Yamaguchi, “Scaling property of the global string in the radiation dominated universe,” *Phys. Rev. D* **60** (1999) 103511, [arXiv:hep-ph/9907506](#).
- [34] M. Yamaguchi, J. Yokoyama, and M. Kawasaki, “Evolution of a global string network in a matter dominated universe,” *Phys. Rev. D* **61** (2000) 061301, [arXiv:hep-ph/9910352](#).
- [35] C. Hagmann, S. Chang, and P. Sikivie, “Axion radiation from strings,” *Phys. Rev. D* **63** (2001) 125018, [arXiv:hep-ph/0012361](#).
- [36] T. Hiramatsu, M. Kawasaki, T. Sekiguchi, M. Yamaguchi, and J. Yokoyama, “Improved estimation of radiated axions from cosmological axionic strings,” *Phys. Rev. D* **83** (2011) 123531, [arXiv:1012.5502 \[hep-ph\]](#).
- [37] T. Hiramatsu, M. Kawasaki, K. Saikawa, and T. Sekiguchi, “Production of dark matter axions from collapse of string-wall systems,” *Phys. Rev. D* **85** (2012) 105020, [arXiv:1202.5851 \[hep-ph\]](#). [Erratum: *Phys.Rev.D* 86, 089902 (2012)].
- [38] L. Fleury and G. D. Moore, “Axion dark matter: strings and their cores,” *JCAP* **01** (2016) 004, [arXiv:1509.00026 \[hep-ph\]](#).
- [39] V. B. Klaer and G. D. Moore, “How to simulate global cosmic strings with large string tension,” *JCAP* **10** (2017) 043, [arXiv:1707.05566 \[hep-ph\]](#).
- [40] M. Gorghetto, E. Hardy, and G. Villadoro, “Axions from Strings: the Attractive Solution,” *JHEP* **07** (2018) 151, [arXiv:1806.04677 \[hep-ph\]](#).
- [41] M. Kawasaki, T. Sekiguchi, M. Yamaguchi, and J. Yokoyama, “Long-term dynamics of cosmological axion strings,” *PTEP* **2018** no. 9, (2018) 091E01, [arXiv:1806.05566 \[hep-ph\]](#).
- [42] M. Buschmann, J. W. Foster, and B. R. Safdi, “Early-Universe Simulations of the Cosmological Axion,” *Phys. Rev. Lett.* **124** no. 16, (2020) 161103, [arXiv:1906.00967 \[astro-ph.CO\]](#).
- [43] M. Hindmarsh, J. Lizarraga, A. Lopez-Eiguren, and J. Urrestilla, “Scaling Density of Axion Strings,” *Phys. Rev. Lett.* **124** no. 2, (2020) 021301, [arXiv:1908.03522 \[astro-ph.CO\]](#).
- [44] V. B. Klaer and G. D. Moore, “Global cosmic string networks as a function of tension,” *JCAP* **06** (2020) 021, [arXiv:1912.08058 \[hep-ph\]](#).
- [45] M. Gorghetto, E. Hardy, and G. Villadoro, “More axions from strings,” *SciPost Phys.* **10** no. 2, (2021) 050, [arXiv:2007.04990 \[hep-ph\]](#).

- [46] M. Hindmarsh, J. Lizarraga, A. Lopez-Eiguren, and J. Urrestilla, “Approach to scaling in axion string networks,” *Phys. Rev. D* **103** no. 10, (2021) 103534, [arXiv:2102.07723 \[astro-ph.CO\]](#).
- [47] M. Buschmann, J. W. Foster, A. Hook, A. Peterson, D. E. Willcox, W. Zhang, and B. R. Safdi, “Dark matter from axion strings with adaptive mesh refinement,” *Nature Commun.* **13** no. 1, (2022) 1049, [arXiv:2108.05368 \[hep-ph\]](#).
- [48] J. J. Blanco-Pillado, D. Jiménez-Aguilar, J. M. Queiruga, and J. Urrestilla, “Parametric Resonances in Axionic Cosmic Strings,” [arXiv:2212.06194 \[hep-th\]](#).
- [49] T. Vachaspati and A. Vilenkin, “Gravitational Radiation from Cosmic Strings,” *Phys. Rev. D* **31** (1985) 3052.
- [50] D. Garfinkle and T. Vachaspati, “Radiation From Kinky, Cuspless Cosmic Loops,” *Phys. Rev. D* **36** (1987) 2229.
- [51] R. R. Caldwell and B. Allen, “Cosmological constraints on cosmic string gravitational radiation,” *Phys. Rev. D* **45** (1992) 3447–3468.
- [52] R. R. Caldwell, R. A. Battye, and E. P. S. Shellard, “Relic gravitational waves from cosmic strings: Updated constraints and opportunities for detection,” *Phys. Rev. D* **54** (1996) 7146–7152, [arXiv:astro-ph/9607130](#).
- [53] T. Damour and A. Vilenkin, “Gravitational wave bursts from cosmic strings,” *Phys. Rev. Lett.* **85** (2000) 3761–3764, [arXiv:gr-qc/0004075](#).
- [54] T. Damour and A. Vilenkin, “Gravitational wave bursts from cusps and kinks on cosmic strings,” *Phys. Rev. D* **64** (2001) 064008, [arXiv:gr-qc/0104026](#).
- [55] T. Damour and A. Vilenkin, “Gravitational radiation from cosmic (super)strings: Bursts, stochastic background, and observational windows,” *Phys. Rev. D* **71** (2005) 063510, [arXiv:hep-th/0410222](#).
- [56] X. Siemens, V. Mandic, and J. Creighton, “Gravitational wave stochastic background from cosmic (super)strings,” *Phys. Rev. Lett.* **98** (2007) 111101, [arXiv:astro-ph/0610920](#).
- [57] M. R. DePies and C. J. Hogan, “Stochastic Gravitational Wave Background from Light Cosmic Strings,” *Phys. Rev. D* **75** (2007) 125006, [arXiv:astro-ph/0702335](#).
- [58] S. Olmez, V. Mandic, and X. Siemens, “Gravitational-Wave Stochastic Background from Kinks and Cusps on Cosmic Strings,” *Phys. Rev. D* **81** (2010) 104028, [arXiv:1004.0890 \[astro-ph.CO\]](#).

- [59] P. Binetruy, A. Bohe, C. Caprini, and J.-F. Dufaux, “Cosmological Backgrounds of Gravitational Waves and eLISA/NGO: Phase Transitions, Cosmic Strings and Other Sources,” *JCAP* **06** (2012) 027, [arXiv:1201.0983 \[gr-qc\]](#).
- [60] S. Kuroyanagi, K. Miyamoto, T. Sekiguchi, K. Takahashi, and J. Silk, “Forecast constraints on cosmic string parameters from gravitational wave direct detection experiments,” *Phys. Rev. D* **86** (2012) 023503, [arXiv:1202.3032 \[astro-ph.CO\]](#).
- [61] S. Kuroyanagi, K. Miyamoto, T. Sekiguchi, K. Takahashi, and J. Silk, “Forecast constraints on cosmic strings from future CMB, pulsar timing and gravitational wave direct detection experiments,” *Phys. Rev. D* **87** no. 2, (2013) 023522, [arXiv:1210.2829 \[astro-ph.CO\]](#). [Erratum: *Phys.Rev.D* 87, 069903 (2013)].
- [62] C. Ringeval and T. Suyama, “Stochastic gravitational waves from cosmic string loops in scaling,” *JCAP* **12** (2017) 027, [arXiv:1709.03845 \[astro-ph.CO\]](#).
- [63] Y. Cui, M. Lewicki, D. E. Morrissey, and J. D. Wells, “Cosmic Archaeology with Gravitational Waves from Cosmic Strings,” *Phys. Rev. D* **97** no. 12, (2018) 123505, [arXiv:1711.03104 \[hep-ph\]](#).
- [64] Y. Gouttenoire, G. Servant, and P. Simakachorn, “Beyond the Standard Models with Cosmic Strings,” *JCAP* **07** (2020) 032, [arXiv:1912.02569 \[hep-ph\]](#).
- [65] M. Gorghetto, E. Hardy, and H. Nicolaescu, “Observing invisible axions with gravitational waves,” *JCAP* **06** (2021) 034, [arXiv:2101.11007 \[hep-ph\]](#).
- [66] C.-F. Chang and Y. Cui, “Gravitational waves from global cosmic strings and cosmic archaeology,” *JHEP* **03** (2022) 114, [arXiv:2106.09746 \[hep-ph\]](#).
- [67] J. J. Blanco-Pillado and K. D. Olum, “Form of cosmic string cusps,” *Phys. Rev. D* **59** (1999) 063508, [arXiv:gr-qc/9810005](#). [Erratum: *Phys.Rev.D* 103, 029902 (2021)].
- [68] K. D. Olum and J. J. Blanco-Pillado, “Field theory simulation of Abelian Higgs cosmic string cusps,” *Phys. Rev. D* **60** (1999) 023503, [arXiv:gr-qc/9812040](#).
- [69] M. Hindmarsh, J. Lizarraga, J. Urrestilla, D. Daverio, and M. Kunz, “Scaling from gauge and scalar radiation in Abelian Higgs string networks,” *Phys. Rev. D* **96** no. 2, (2017) 023525, [arXiv:1703.06696 \[astro-ph.CO\]](#).
- [70] D. Matsunami, L. Pogosian, A. Saurabh, and T. Vachaspati, “Decay of Cosmic String Loops Due to Particle Radiation,” *Phys. Rev. Lett.* **122** no. 20, (2019) 201301, [arXiv:1903.05102 \[hep-ph\]](#).
- [71] A. Saurabh, T. Vachaspati, and L. Pogosian, “Decay of Cosmic Global String Loops,” *Phys. Rev. D* **101** no. 8, (2020) 083522, [arXiv:2001.01030 \[hep-ph\]](#).

- [72] R. Jeannerot, X. Zhang, and R. H. Brandenberger, “Non-thermal production of neutralino cold dark matter from cosmic string decays,” *JHEP* **12** (1999) 003, [arXiv:hep-ph/9901357](#).
- [73] Y. Cui, S. P. Martin, D. E. Morrissey, and J. D. Wells, “Cosmic Strings from Supersymmetric Flat Directions,” *Phys. Rev. D* **77** (2008) 043528, [arXiv:0709.0950 \[hep-ph\]](#).
- [74] Y. Cui and D. E. Morrissey, “Non-Thermal Dark Matter from Cosmic Strings,” *Phys. Rev. D* **79** (2009) 083532, [arXiv:0805.1060 \[hep-ph\]](#).
- [75] M. Kawasaki, K. Miyamoto, and K. Nakayama, “Cosmological Effects of Decaying Cosmic String Loops with TeV Scale Width,” [arXiv:1105.4383 \[hep-ph\]](#).
- [76] K. Miyamoto and K. Nakayama, “Cosmological and astrophysical constraints on superconducting cosmic strings,” *JCAP* **07** (2013) 012, [arXiv:1212.6687 \[astro-ph.CO\]](#).
- [77] M. Hindmarsh and J. Kume, “Multi-messenger constraints on Abelian-Higgs cosmic string networks,” [arXiv:2210.06178 \[astro-ph.CO\]](#).
- [78] J. N. Moore, E. P. S. Shellard, and C. J. A. P. Martins, “On the evolution of Abelian-Higgs string networks,” *Phys. Rev. D* **65** (2002) 023503, [arXiv:hep-ph/0107171](#).
- [79] N. Bevis, M. Hindmarsh, M. Kunz, and J. Urrestilla, “CMB power spectrum contribution from cosmic strings using field-evolution simulations of the Abelian Higgs model,” *Phys. Rev. D* **75** (2007) 065015, [arXiv:astro-ph/0605018](#).
- [80] J.-F. Dufaux, D. G. Figueroa, and J. Garcia-Bellido, “Gravitational Waves from Abelian Gauge Fields and Cosmic Strings at Preheating,” *Phys. Rev. D* **82** (2010) 083518, [arXiv:1006.0217 \[astro-ph.CO\]](#).
- [81] T. Hiramatsu, Y. Sendouda, K. Takahashi, D. Yamauchi, and C.-M. Yoo, “Type-I cosmic string network,” *Phys. Rev. D* **88** no. 8, (2013) 085021, [arXiv:1307.0308 \[astro-ph.CO\]](#).
- [82] J. R. C. C. Correia and C. J. A. P. Martins, “Abelian-Higgs Cosmic String Evolution with CUDA,” *Astron. Comput.* **32** (2020) 100388, [arXiv:1809.00995 \[physics.comp-ph\]](#).
- [83] J. R. C. C. C. Correia and C. J. A. P. Martins, “Abelian-Higgs cosmic string evolution with multiple GPUs,” *Astron. Comput.* **34** (2021) 100438, [arXiv:2005.14454 \[physics.comp-ph\]](#).

- [84] K. Kajantie, M. Karjalainen, M. Laine, J. Peisa, and A. Rajantie, “Thermodynamics of gauge invariant U(1) vortices from lattice Monte Carlo simulations,” *Phys. Lett. B* **428** (1998) 334–341, [arXiv:hep-ph/9803367](#).
- [85] M. Kawasaki, K. Miyamoto, and K. Nakayama, “Gravitational waves from kinks on infinite cosmic strings,” *Phys. Rev. D* **81** (2010) 103523, [arXiv:1002.0652](#) [[astro-ph.CO](#)].
- [86] Y. Matsui, K. Horiguchi, D. Nitta, and S. Kuroyanagi, “Improved calculation of the gravitational wave spectrum from kinks on infinite cosmic strings,” *JCAP* **11** (2016) 005, [arXiv:1605.08768](#) [[astro-ph.CO](#)].
- [87] Y. Matsui and S. Kuroyanagi, “Gravitational wave background from kink-kink collisions on infinite cosmic strings,” *Phys. Rev. D* **100** no. 12, (2019) 123515, [arXiv:1902.09120](#) [[astro-ph.CO](#)].
- [88] K. Saikawa and S. Shirai, “Primordial gravitational waves, precisely: The role of thermodynamics in the Standard Model,” *JCAP* **05** (2018) 035, [arXiv:1803.01038](#) [[hep-ph](#)].
- [89] **LIGO Scientific, Virgo** Collaboration, B. P. Abbott *et al.*, “Constraints on cosmic strings using data from the first Advanced LIGO observing run,” *Phys. Rev. D* **97** no. 10, (2018) 102002, [arXiv:1712.01168](#) [[gr-qc](#)].
- [90] **LIGO Scientific** Collaboration, J. Aasi *et al.*, “Advanced LIGO,” *Class. Quant. Grav.* **32** (2015) 074001, [arXiv:1411.4547](#) [[gr-qc](#)].
- [91] **VIRGO** Collaboration, F. Acernese *et al.*, “Advanced Virgo: a second-generation interferometric gravitational wave detector,” *Class. Quant. Grav.* **32** no. 2, (2015) 024001, [arXiv:1408.3978](#) [[gr-qc](#)].
- [92] M. Punturo *et al.*, “The Einstein Telescope: A third-generation gravitational wave observatory,” *Class. Quant. Grav.* **27** (2010) 194002.
- [93] N. Bartolo *et al.*, “Science with the space-based interferometer LISA. IV: Probing inflation with gravitational waves,” *JCAP* **12** (2016) 026, [arXiv:1610.06481](#) [[astro-ph.CO](#)].
- [94] K. Yagi and N. Seto, “Detector configuration of DECIGO/BBO and identification of cosmological neutron-star binaries,” *Phys. Rev. D* **83** (2011) 044011, [arXiv:1101.3940](#) [[astro-ph.CO](#)]. [Erratum: *Phys.Rev.D* 95, 109901 (2017)].
- [95] R. van Haasteren *et al.*, “Placing limits on the stochastic gravitational-wave background using European Pulsar Timing Array data,” *Mon. Not. Roy. Astron. Soc.* **414** no. 4, (2011) 3117–3128, [arXiv:1103.0576](#) [[astro-ph.CO](#)]. [Erratum: *Mon.Not.Roy.Astron.Soc.* 425, 1597 (2012)].

- [96] **NANOGrav** Collaboration, Z. Arzoumanian *et al.*, “The NANOGrav 12.5 yr Data Set: Search for an Isotropic Stochastic Gravitational-wave Background,” *Astrophys. J. Lett.* **905** no. 2, (2020) L34, [arXiv:2009.04496](https://arxiv.org/abs/2009.04496) [astro-ph.HE].
- [97] G. Janssen *et al.*, “Gravitational wave astronomy with the SKA,” *PoS AASKA14* (2015) 037, [arXiv:1501.00127](https://arxiv.org/abs/1501.00127) [astro-ph.IM].
- [98] K. Schmitz, “New Sensitivity Curves for Gravitational-Wave Signals from Cosmological Phase Transitions,” *JHEP* **01** (2021) 097, [arXiv:2002.04615](https://arxiv.org/abs/2002.04615) [hep-ph].
- [99] K. Schmitz, “New Sensitivity Curves for Gravitational-Wave Experiments (Version v1) [Data set],” <https://doi.org/10.5281/zenodo.3689582> (2020) .